



2013

13th Oxford Summer School on Neutron Scattering

Exercise Book

Useful Physical Constants	1
A) Coherent and Incoherent Scattering	2
B) Time-of-flight Powder Diffraction	5
C) Single Crystal Diffraction	10
D) Incoherent Inelastic Scattering	13
E) Coherent Inelastic Scattering	15
F) Magnetic Scattering	21
G) Disordered Materials Scattering	23
H) Polarized Neutrons	30
I) High Resolution Spectroscopy	33

The school is supported by:



Science & Technology Facilities Council
ISIS



<http://www.oxfordneutronschool.org>

2nd – 13th September 2013

Values of Physical Constants

Constant	Symbol	SI Units	“Neutron” Units
Speed of light	c	$3.00 \times 10^8 \text{ m s}^{-1}$	
Electron charge	e	$1.60 \times 10^{-19} \text{ C}$	
Boltzmann's constant	k_B	$1.38 \times 10^{-23} \text{ J K}^{-1}$	0.086 meV K^{-1}
Planck's constant	h	$6.63 \times 10^{-34} \text{ J s}$	$4.14 \times 10^{-12} \text{ meV s}$
	$\hbar = h/2\pi$	$1.06 \times 10^{-34} \text{ J s}$	$6.58 \times 10^{-13} \text{ meV s}$
Avogadro's number	N_A	$6.02 \times 10^{23} \text{ mol}^{-1}$	
Mass of electron	m_e	$9.11 \times 10^{-31} \text{ kg}$	
Mass of proton	m_p	$1.67 \times 10^{-27} \text{ kg}$	
Bohr magneton	$\mu_B = \frac{e\hbar}{2m_e}$	$9.274 \times 10^{-24} \text{ J/T}$	
Nuclear magneton	$\mu_N = \frac{e\hbar}{2m_p}$	$5.051 \times 10^{-27} \text{ J/T}$	

Properties of the neutron

mass m_n	$1.67 \times 10^{-27} \text{ kg}$
charge	0
spin	1/2
magnetic moment	$-1.913 \mu_N$

Relations between Units

$$1 \text{ meV} = 1.6 \times 10^{-22} \text{ J} = 0.24 \text{ THz} = 8.1 \text{ cm}^{-1} = 11.6 \text{ K}$$

A. Coherent and Incoherent Scattering

These exercises illustrate how to calculate coherent scattering amplitudes and incoherent scattering cross sections for nuclear scattering

Formulae

A neutron of spin $\frac{1}{2}$ interacts with a nucleus of spin I to form two states in which the spins are either parallel or antiparallel. The combined spin J of these states is $J = I + \frac{1}{2}$ and $J = I - \frac{1}{2}$, respectively. Different scattering lengths (amplitudes) b^+ , b^- are associated with these states. The probabilities (statistical weights) w^+ , w^- of the states are proportional to the number of spin orientations of each state. This number is $2J + 1$, so $w^+ \propto 2I + 2$ and $w^- \propto 2I$. By constraining $w^+ + w^- = 1$, we find

$$w^+ = \frac{I+1}{2I+1} w^+ = \frac{I+1}{2I+1} \quad \text{and} \quad w^- = \frac{I}{2I+1} \quad (\text{A1})$$

Suppose that an atom has several isotopes and that the spin of the r^{th} isotope is I_r . The **coherent scattering length** b_{coh} of the atom is the scattering length averaged over all the isotopes and spin states, i.e.

$$b_{\text{coh}} = \bar{b} = \sum_r c_r (w_r^+ b_r^+ + w_r^- b_r^-) \quad (\text{A2})$$

where c_r is the abundance of isotope r , and w_r^+ and w_r^- are given by (A1) with I replaced by I_r .

We define the single-atom **coherent scattering cross section** by

$$\sigma_{\text{coh}} = 4\pi b_{\text{coh}}^2 = 4\pi \bar{b}^2 \quad (\text{A3})$$

The single-atom **total scattering cross section** is obtained by averaging the separate cross sections for each of the individual isotopes r in both possible spin states:

$$\begin{aligned} \sigma_{\text{tot}} &= 4\pi \sum_r c_r \{w_r^+ (b_r^+)^2 + w_r^- (b_r^-)^2\} \\ &= 4\pi \overline{b^2} \end{aligned} \quad (\text{A4})$$

Finally, the single-atom **incoherent scattering cross section** is the difference between the total and coherent cross sections:

$$\begin{aligned} \sigma_{\text{inc}} &= \sigma_{\text{tot}} - \sigma_{\text{coh}} \\ &= 4\pi (\overline{b^2} - \bar{b}^2) \end{aligned} \quad (\text{A5})$$

Exercises

A1 Table A.1 gives the nuclear spin I of the two most abundant isotopes of hydrogen, ^1H (protium) and ^2H (deuterium), together with the measured scattering lengths of the (neutron + nucleus) systems with combined spins $I + \frac{1}{2}$ and $I - \frac{1}{2}$. Calculate σ_{coh} and σ_{inc} for ^1H and ^2H .

Table A.1.

	spin I	b^+ (fm)	b^- (fm)
^1H (protium)	$\frac{1}{2}$	10.82	-47.4
^2H (deuterium)	1	9.53	0.98

$$1 \text{ fm} = 10^{-15} \text{ m}$$

You should find that σ_{coh} for ^1H and ^2H are quite different. This means that the scattering from certain parts of a hydrogen-containing sample can be enhanced through selective replacement of the hydrogen atoms by deuterium, a process known as *isotopic labelling*.

You should also find that σ_{inc} for ^1H is much larger than that of ^2H , so that σ_{inc} for natural hydrogen is close to that of ^1H (natural hydrogen is 99.99% ^1H). Hence, neutron scatterers often try to minimise the amount of hydrogen-containing materials (like glue) in the neutron beam during their experiments. If hydrogen is present in the sample itself, then the background can be considerably reduced if the sample is prepared with deuterium instead of hydrogen.

A2 Table A.2 gives the experimental values of the scattering lengths and the abundance of the individual isotopes of nickel: ^{58}Ni , ^{60}Ni , ^{61}Ni , ^{62}Ni and ^{64}Ni . With the exception of ^{61}Ni , the isotopes have zero spin and so b^+ is the same as b^- . Calculate the values of σ_{coh} and σ_{inc} for a natural nickel sample containing all five isotopes.

Table B.2.

Abundances, nuclear spins and scattering lengths of the isotopes of nickel

Isotope, r	abundance c_r	spin I_r	b_r^+ (fm)	b_r^- (fm)
58	68.3%	0	14.4	14.4
60	26.1%	0	2.8	2.8
61	1.1%	3/2	4.6	12.6
62	3.6%	0	-8.7	-8.7
64	0.9%	0	-0.4	-0.4

B. Time-of-Flight Powder Diffraction

B1.

(a) In a time-of-flight powder diffraction experiment the incident beam is pulsed, and with each pulse a polychromatic burst of neutrons strikes the sample. The different wavelengths, λ , in a pulse are separated by measuring their time-of-flight (t.o.f.), t , from source to detector. Using the table of physical constants at the back, show that the relation between wavelength and t.o.f. is given by

$$t \text{ (}\mu\text{secs)} = 252.8 \times \lambda \text{ (}\text{\AA}) \times L \text{ (m)}$$

where L is the total flight path between the source and detector.

(b) A powder diffractometer, with total flight path $L = 100$ m and scattering angle $2\theta = 170^\circ$, was used to obtain the powder diffraction pattern of perovskite, CaTiO_3 . Calculate the values of t for the three Bragg reflections with the longest times of flight. (CaTiO_3 crystallises in a primitive cubic lattice with a unit cell of edge $a_0 = 3.84 \text{ \AA}$.)

(c) For a sample with a cubic unit cell, show that the time-of-flight t of each Bragg peak in the t.o.f. powder diffraction pattern is related to its indices H, K, L by:

$$t \propto (H^2 + K^2 + L^2)^{-1/2} \quad (\text{B1})$$

B2.

Silicon crystallises in the face-centred-cubic (fcc) structure of diamond with the lattice points at:

$$0, 0, 0; \quad \frac{1}{2}, \frac{1}{2}, 0; \quad \frac{1}{2}, 0, \frac{1}{2}; \quad 0, \frac{1}{2}, \frac{1}{2}$$

In this structure there is a primitive basis of two identical atoms at $0,0,0$ and $\frac{1}{4}, \frac{1}{4}, \frac{1}{4}$ which is associated with each lattice point of the unit cell.

(a) Show that the Millar indices H, K, L of the Bragg reflections for the fcc lattice are all odd or all even.

(b) Show that reflections with an odd value of $(H + K + L)/2$ such as (222) and (442), are forbidden in this structure.

(c) From eqn. (B1) the Bragg reflections in the powder diffraction pattern are separated according to their values of $(H^2 + K^2 + L^2)$. In table B.1 all the possible values of $(H^2 + K^2 + L^2)$ are listed in the order of decreasing time-of-flight in the range;

$$3 \leq (H^2 + K^2 + L^2) \leq 40$$

(This is the range covered in Figure B1)

Table B1.

Sums of three squared integers.

$H^2+K^2+L^2$	$H^2+K^2+L^2$	$H^2+K^2+L^2$	$H^2+K^2+L^2$
3*	12*	21	32*
4*	13	22	33
5	14	24*	34
6	16*	25	35*
8*	17	26	36*
9	18	27*	37
10	19*	29	38
11*	20*	30	40*

The values of $(H^2+K^2+L^2)$ in which the integers are all odd or all even are marked with asterisks.

- (i) What are the indices H, K, L , corresponding to these asterisks?
- (ii) Which of the fcc reflections are forbidden?
- (iii) Which of the allowed fcc reflections overlap with one another?

(d) Figure B1 shows the diffraction pattern of powdered silicon, taken with the time-of-flight diffractometer HRPD at the ISIS pulsed neutron source. The scattering angle was $2\theta = 90.8^\circ$ and the path length $L = 96.8$ m.

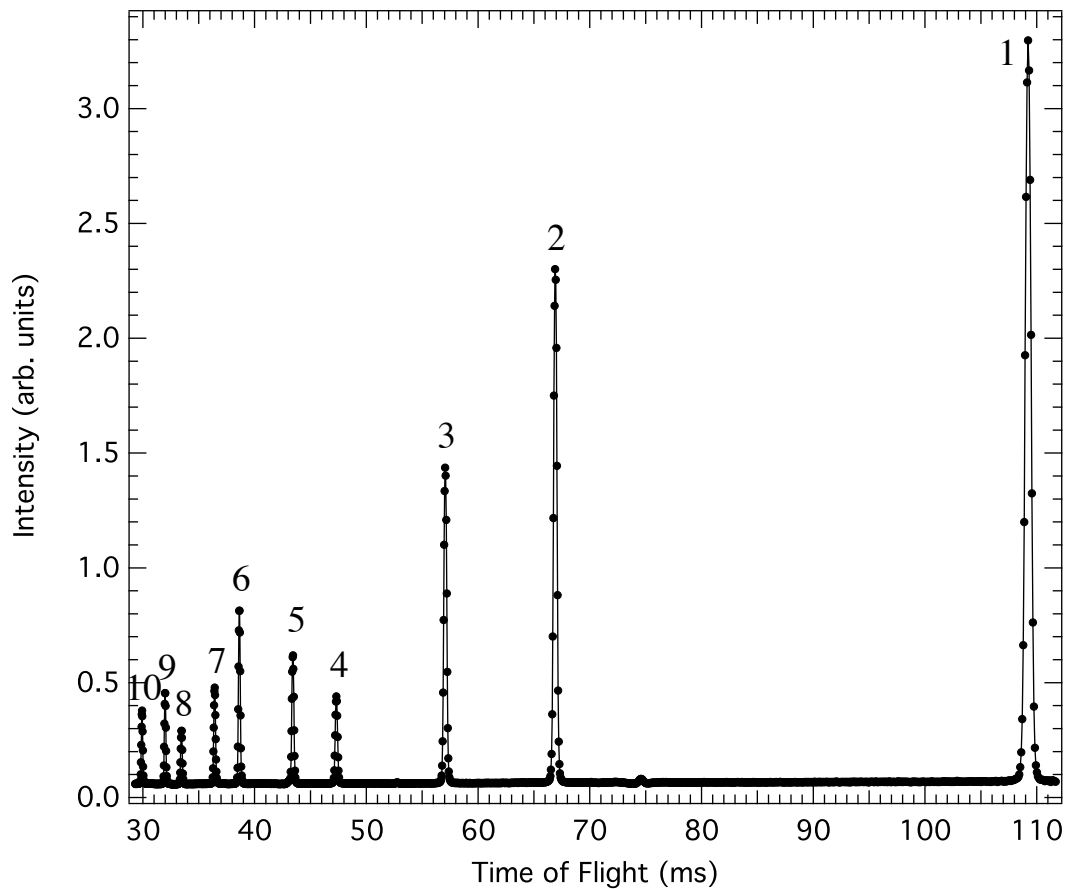


Figure B1. *Time-of-flight diffraction pattern of powdered silicon. The observed spectrum has been normalised to a vanadium spectrum: vanadium is an incoherent scatterer whose spectrum gives the wavelength dependence of the incident neutron flux.*

The values of t for the 10 numbered Bragg peaks in Figure B1 were measured (to a precision of better than 1 part in 10^5) giving the results in Table B2.

Index all these peaks and determine the linear size a_0 of the unit cell of silicon.

The position of the first peak appears to be shifted to lower time-of-flight than expected. Any ideas why?

Table B2

peak number	time of flight (ms)
1	109.232
2	66.912
3	57.066
4	47.320
5	43.424
6	38.636
7	36.426
8	33.457
9	31.991
10	29.923

B3.

In a t.o.f. neutron powder diffractometer, a sharp pulse of neutrons with a range of wavelengths is fired at the sample. The diffracted signal is measured at a fixed scattering angles 2θ , and the diffraction patterns comes about from measurements of the time taken for the neutrons in a single pulse to travel the distance L from the source to the detector. Using the de Broglie relationship together with the Bragg's Law, show that the time t taken by the neutrons to travel the distance L is related to the d -spacing of a given Bragg reflection by

$$d = \frac{ht}{2mL \sin \theta} \quad (\text{B2})$$

where m is the mass of the neutron.

For an uncertainty of $\Delta\theta$ in the scattering angle (caused by beam divergence, or finite sample/detector width), error analysis gives the corresponding uncertainty in the d -spacing:

$$\Delta d = \frac{\partial d}{\partial \theta} \Delta \theta \quad (\text{B3})$$

Show by differentiation of Bragg's law that for a given uncertainty $\Delta\theta$ this leads to a maximum resolution in the d -spacing of

$$\left| \frac{\Delta d}{d} \right| = \cot \theta \Delta \theta \quad (\text{B4})$$

In order to maximize the resolution of a t.o.f. powder diffractometer, the scattering angle 2θ is chosen to be as close to 180° as possible (backscattering detector banks). In this case a significant source of uncertainty is in the distance travelled by the neutron beam. Show that the uncertainty in the flight path L of ΔL leads to a resolution limit of

$$\frac{\Delta d}{d} = \frac{\Delta L}{L} \quad (\text{B5})$$

If the only uncertainty in the value of L comes from the depth of a neutron moderator, 2 cm thick, calculate the flight paths necessary to achieve;

(a) a moderate resolution of $\Delta d/d = 10^{-3}$

(b) a high resolution $\Delta d/d = 2 \times 10^{-4}$

Comment on your answers, and check out the real situation at the ISIS spallation neutron source by looking at the instruments POLARIS and HRPD from <http://www.isis.rl.ac.uk>.

C. Single-Crystal Diffraction

C1.

2.20 km/sec is conventionally taken as a standard velocity for thermal neutrons. (For example, absorption cross sections are tabulated for this value of the velocity.)

(i) Using the de Broglie relation show that the wavelength of neutrons with this standard velocity is approximately 1.8 Å.

(ii) What is the kinetic energy of these neutrons? (See values of physical constants, p1)

(iii) What is the energy of an X-ray photon of wavelength $\lambda = 1.8 \text{ \AA}$?

(iv) Calculate the velocity of a neutron having the same energy as this X-ray photon.

C2.

A beam of “white” neutrons emerges from a collimator with a divergence of $\pm 0.2^\circ$. It is then Bragg reflected by the (111) planes of a monochromator consisting of a single-crystal of lead.

(i) Calculate the angle between the direct beam and the [111] axis of the crystal to produce a beam of wavelength $\lambda = 1.8 \text{ \AA}$. (Unit cell edge a_0 of cubic lead is 4.94 Å)

(ii) What is the spread in wavelengths of the reflected beam?

Questions **C3** and **C4** are concerned with the treatment of Bragg scattering in reciprocal space. **C3** refers to the scattering of neutrons of a fixed-wavelength, and **C4** to the scattering of pulsed neutrons covering a wide band of wavelengths.

C3.

A single crystal has an orthorhombic unit cell with dimensions $a = 6 \text{ \AA}$, $b = 8 \text{ \AA}$ and $c = 10 \text{ \AA}$. Plot the reciprocal lattice in the $\mathbf{a}^*-\mathbf{b}^*$ plane adopting a scale of $1 \text{ \AA}^{-1} = 20 \text{ mm}$.

A horizontal beam of neutrons of wavelength $\lambda = 1.8 \text{ \AA}$ strikes the crystal. The crystal is rotated about its vertical \mathbf{c} axis between the settings for the (630) and (360) Bragg reflections. Draw the Ewald circles for these two reflections. How many $(HK0)$ reflections will give rise to Bragg scattering while the crystal is rotated between (630) and (360) ?

C4.

A pulse of neutrons with a wavelength range from 1.8 \AA to 5.0 \AA undergoes Bragg scattering from this crystal. The neutron beam is parallel to the \mathbf{a} axis of the crystal and strikes the crystal at right angles to the \mathbf{c} axis. Using the Ewald construction find the maximum number of Bragg reflections which could be observed simultaneously in the horizontal scattering plane.

C5.

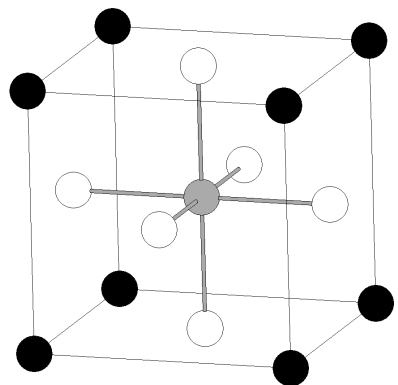


Figure C1

High-temperature cubic phase of BaTiO₃

Ba ²⁺	●	0, 0, 0
Ti ⁴⁺	●	1/2, 1/2, 1/2
O ²⁻	○	1/2, 1/2, 0; 1/2, 0, 1/2; 0, 1/2, 1/2

(i) The diagram shows the high-temperature cubic unit cell of BaTiO₃ alongside a list of the fractional coordinates of the ions in the unit cell. Show that the intensity $I_{(00L)}$ of the neutron beam diffracted from the $(00L)$ planes of cubic BaTiO₃ is proportional to

$$[b_{\text{Ba}} + (-1)^L b_{\text{Ti}} + (1 + 2(-1)^L)b_{\text{O}}]^2,$$

where b_{Ba} , b_{Ti} and b_{O} are the coherent scattering lengths of the nuclei.

(ii) On cooling through the ferroelectric transition temperature $T_c = 130$ C the structure of BaTiO_3 undergoes a displacive transition in which the Ti^{4+} and O^{2-} ions move in opposite directions relative to the Ba^{2+} ions. As a first approximation the fractional coordinates of the ions in the distorted phase are

$$\begin{array}{ll} \text{Ba}^{2+} & 0, 0, 0 \\ \text{Ti}^{4+} & \frac{1}{2}, \frac{1}{2}, \frac{1}{2} + \delta \\ \text{O}^{2-} & \frac{1}{2}, \frac{1}{2}, -\delta; \quad \frac{1}{2}, 0, \frac{1}{2} - \delta; \quad 0, \frac{1}{2}, \frac{1}{2} - \delta, \end{array}$$

where $\delta \ll 1$.

The intensity of the (005) neutron diffraction peak from a single crystal of BaTiO_3 is found to increase by 74% on cooling the crystal through T_c . Use this observation to determine δ .

(iii) Explain why it is advantageous to use neutron diffraction, rather than X-ray diffraction, to determine the ionic displacements. (Assume that the X-ray atomic scattering factors, f , for the (005) reflection are proportional to the atomic number Z .)

Coherent scattering lengths:

$$\begin{array}{ll} b_{\text{Ba}} & = \quad 5.25 \times 10^{-15} \text{ m} \\ b_{\text{Ti}} & = \quad -3.30 \times 10^{-15} \text{ m} \\ b_{\text{O}} & = \quad 5.81 \times 10^{-15} \text{ m} \end{array}$$

atomic numbers:

$$\begin{array}{ll} Z_{\text{Ba}} & = \quad 56 \\ Z_{\text{Ti}} & = \quad 22 \\ Z_{\text{O}} & = \quad 8 \end{array}$$

D. Incoherent Inelastic Scattering **(with a Pulsed Neutron Spectrometer)**

IRIS is an "inverted-geometry" spectrometer, which is installed at the pulsed neutron source ISIS. A white beam of neutrons strikes the sample, and is scattered to the pyrolytic-graphite analyser. The 002 planes of the analyser Bragg reflect the neutrons to the detector. The distance from the moderator to the sample is 36.54 m, and the distance sample-to-analyser-to-detector is 1.47 m. (See Figure D1.)

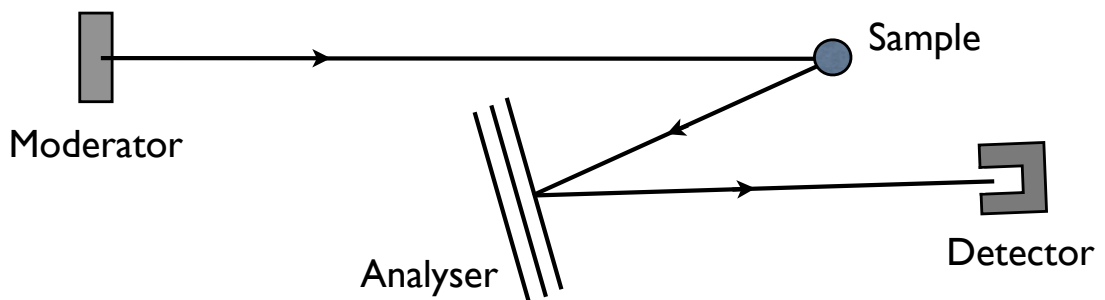


Figure D1. *Geometry of the IRIS spectrometer.*

The IRIS spectrum shown in Figure D2 is for a sample of ammonia intercalated between the layers of oriented graphite. The central peak corresponds to elastic scattering by the sample, and the two outer peaks arise from inelastic scattering due to the tunnelling of hydrogen atoms between adjacent potential wells of the ammonia molecule.

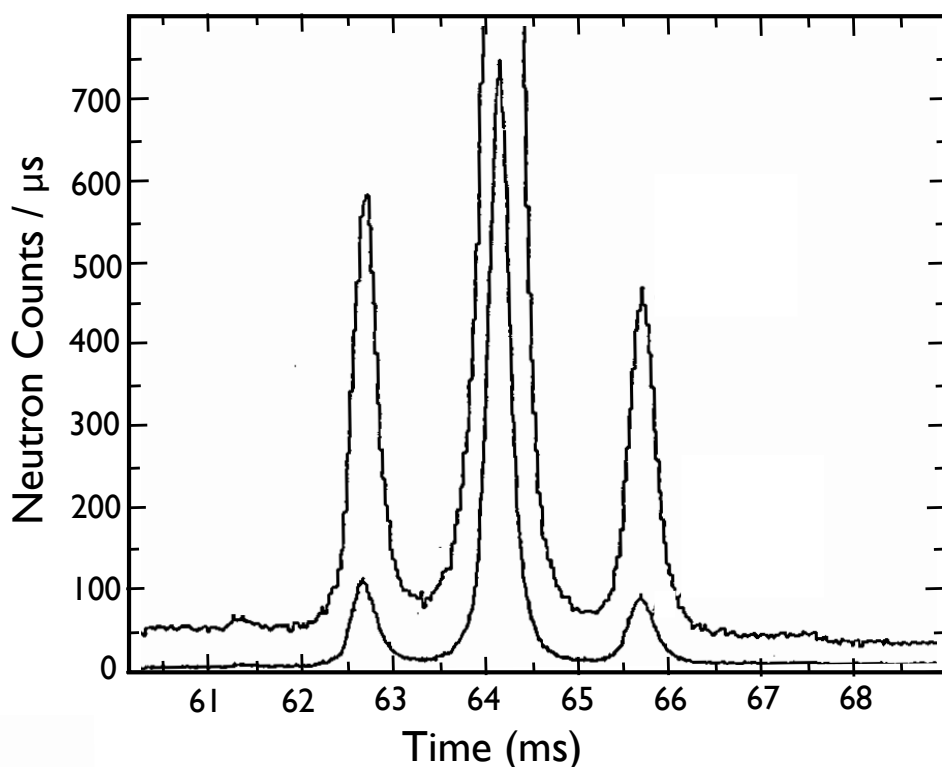


Figure D2. *Time-of-flight spectrum of ammonia intercalated in graphite, measured on IRIS*

D1.

- (i) What is the energy selected by the crystal analyser ?
- (ii) The d -spacing of the (002) planes in pyrolytic graphite is 3.35 \AA . What is the Bragg angle θ_A of the analyser?
- (iii) What is the advantage of using such a high take-off angle $2\theta_A$ for the analyser?

D2.

Identify the peaks in the spectrum which are associated with energy gain and with energy loss. What is the magnitude of the energy transfer for these peaks ?

D3.

- (i) Why are the intensities of the energy-gain and energy-loss peaks different?
- (ii) What does this difference tell us about the temperature of the sample?

E. Coherent Inelastic Scattering (with a Three-Axis Spectrometer)

One of the most important instruments used in neutron scattering is the three-axis spectrometer. A schematic drawing of the machine is shown in Figure E1. By employing a monochromatic neutron beam of a definite wave-vector \mathbf{k}_i (of magnitude $k_i = 2\pi / \lambda_i$ with λ_i the incident wavelength), which is incident on a single crystal in a known orientation, and by measuring the final wave-vector \mathbf{k}_f after scattering by the sample, we can examine excitations such as phonons (in which the atoms are excited by thermal vibrations) or magnons (in which the spin system of the atom is excited).

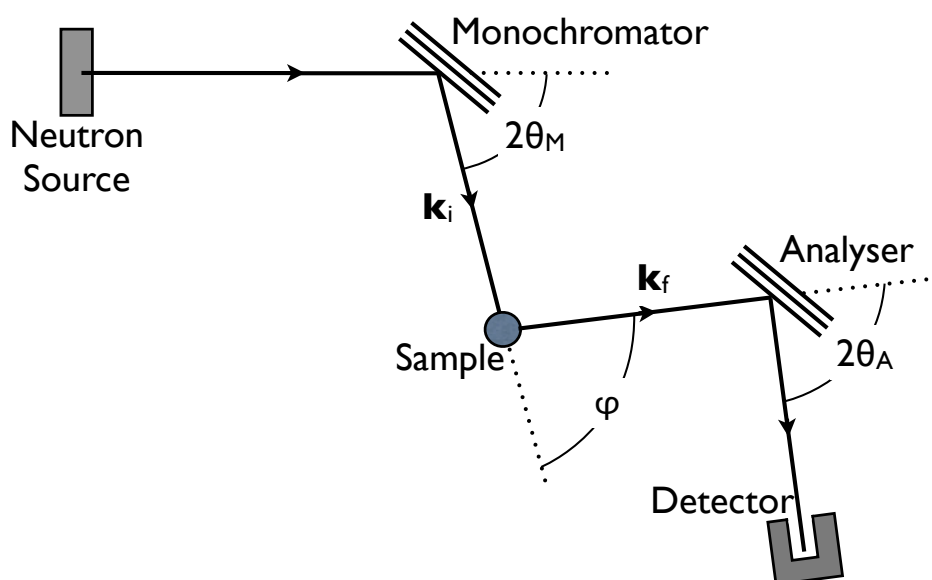


Figure E1. *Three-axis spectrometer.*

The three-axis instrument appears to be complicated, but it is conceptually simple and every movement may be mapped by considering the so-called scattering triangle (Figure E2). In practice, what is difficult about a three-axis machine is that there are many different ways of performing an experiment, and choosing the appropriate configuration is often the key to performing a successful experiment. This is in contrast to a powder diffraction experiment, where one simply puts the sample in the beam and records the diffraction pattern. (See Section B).

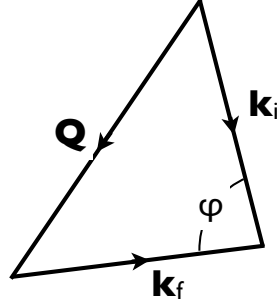


Figure E2. Scattering triangle representing the momentum $\hbar Q$ transferred to the sample when the wavevector of the neutron changes from k_i to k_f . ϕ is the scattering angle.

In the following we shall consider how one actually measures a phonon excitation, using various diagrams in reciprocal space to represent the process. We use formulae which apply to all scattering processes (both neutrons and X-rays).

Momentum conservation gives

$$\mathbf{Q} = \mathbf{k}_i - \mathbf{k}_f \quad (\text{E1})$$

where \mathbf{Q} is the scattering vector. If ϕ is the angle between \mathbf{k}_i and \mathbf{k}_f , we have

$$Q^2 = k_i^2 + k_f^2 - 2 k_i k_f \cos \phi \quad (\text{E2})$$

Energy conservation gives

$$\Delta E = E_i - E_f \quad (\text{E3})$$

where E_i is the energy of the incident neutron, E_f is its energy after scattering, and ΔE is the energy transferred to the scattering system. ΔE may be positive (neutrons lose energy) or negative (neutrons gain energy). If k is the wave-number of a neutron, its energy E is related to k by

$$E = 81.8 / \lambda^2 = 2.072 k^2 \quad (\text{E4})$$

where E is in meV, λ is in \AA and k is in \AA^{-1} .

For the following exercises, imagine that you wish to investigate the low-energy spectra of silver chloride, AgCl, which is a cubic crystal with a face-centred cubic unit cell. You have been allocated time on a three-axis spectrometer, which works with incident neutrons of energy from 3 to 14 meV.

Figure E3 shows the (HHL) plane of reciprocal space. The cubic lattice parameter a_0 of AgCl is 5.56 Å. One reciprocal lattice unit (r.l.u.) is equal to $2\pi / a_0$ or 1.13 \AA^{-1} . The vector from the origin to any point HKL of the reciprocal lattice is of length, $2\pi / d_{\text{HKL}}$ where d_{HKL} is the spacing of the (HKL) planes in the real-space lattice.

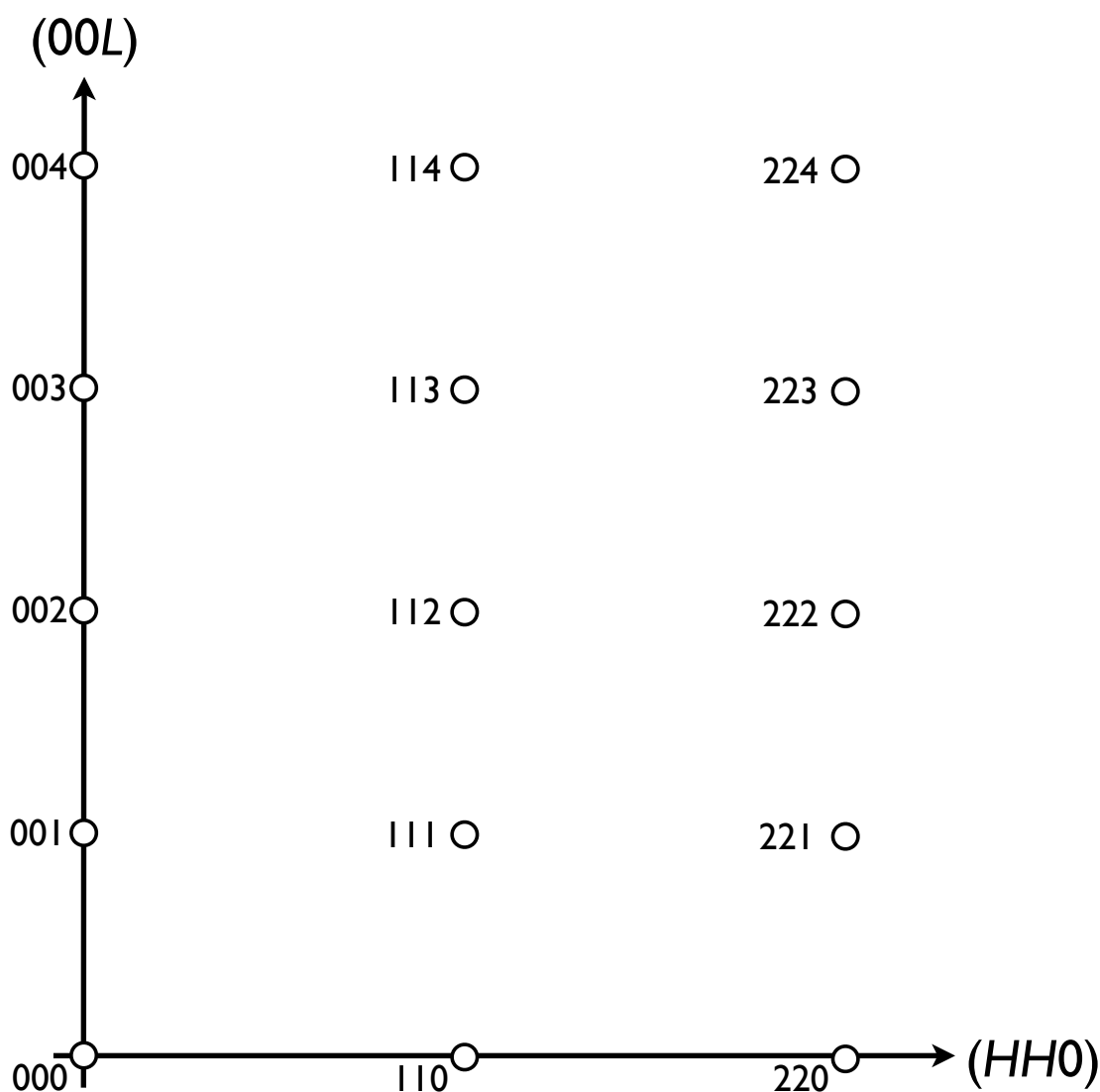


Figure E3. (HHL) plane in reciprocal space of cubic crystal.

F1

Which are the allowed points (giving non-zero Bragg reflections) of the reciprocal lattice in Figure E3? Mark them with a filled-in circle—they are the so-called zone-centres of the Brillouin zone. Leave the disallowed points as open points—these are the zone-boundaries of the Brillouin zone. (Note that the reciprocal lattice of a face-centred cubic crystal is a body-centred cubic lattice.)

F2

E_i ranges from 3 to 14 meV. Calculate the maximum and minimum values of the wavelength λ_i and the wave number k_i of the incident beam.

F3.

We shall begin our experiment using the maximum value of k_i and orienting our crystal to find the 220 Bragg reflection. The scattering we observe is elastic scattering, which is much stronger than the inelastic scattering.

(i) What is the magnitude of $Q_{220} = 2\pi / d_{220}$
Draw \mathbf{Q} , \mathbf{k}_i and \mathbf{k}_f for the 220 reflection.

(ii) What is the angle ϕ between \mathbf{k}_i and \mathbf{k}_f ?

(iii) What is the relation between the Bragg angle θ_B at the sample and ϕ ?

F4.

We can now start our inelastic experiment. Consider the dispersion curves for AgCl shown in Figure E4. Let us suppose that we wish to measure the phonon with a reduced wave vector of 0.4 propagating in the $[00L]$ direction and that the phonon is transverse acoustic. (A shorthand notation for this is TA $[00L]$.) Using the conversion constants on p1 we see that the energy of this phonon is about 3meV.

In Figure E3 draw the wave-vector \mathbf{q} of this phonon away from the 220 zone-centre. (By zone-centre we mean $q = 0$)

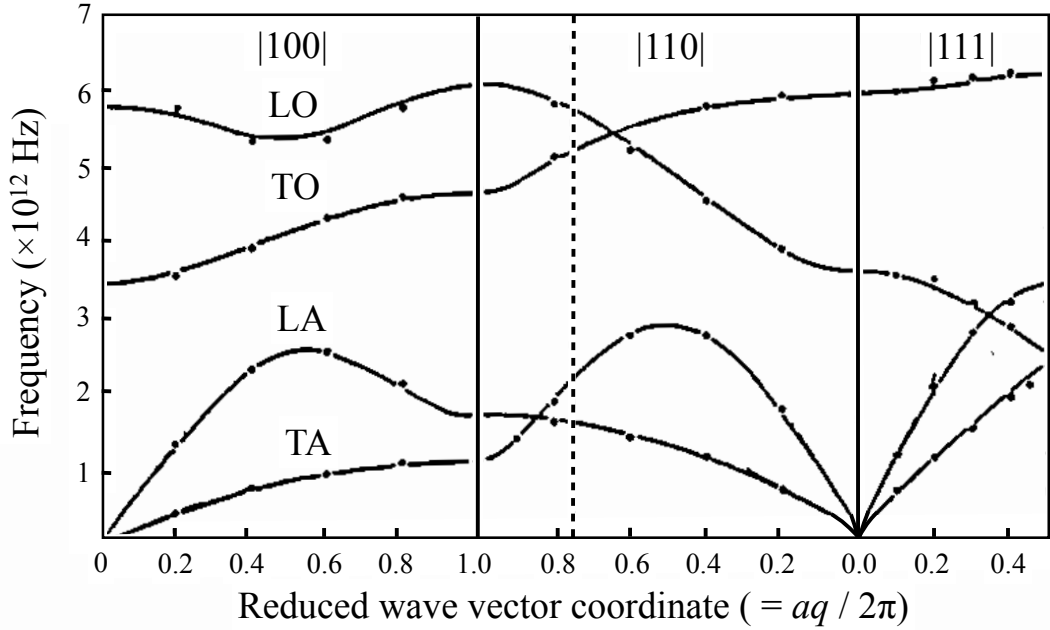


Figure E4. Phonon dispersion curves of cubic AgCl.

We will perform our experiment by using the maximum value of k_i .

E5.

Work out the possible values of k_f and ϕ . (There are two solutions depending on whether ΔE which is the phonon energy, is chosen to be positive or negative.)

E6.

It turns out that better resolution occurs for energy loss than for energy gain. Draw the configuration of k_i and k_f in Figure F3 for energy loss.

Another factor influencing the intensity which we observe in our experiment is the so-called Bose factor $n(E)$. This gives the population of phonon states at any given energy and temperature:

$$n(E) = \frac{1}{\exp(E/k_B T) - 1}$$

The intensity for neutron energy loss is proportional to $[1 + n(E)]$, whereas for neutron energy gain it is proportional to $n(E)$.

E7.

- (i) Calculate the Bose factors for the energy gain and energy loss configurations in our example assuming that the sample is at a temperature of: (a) 300 K, (b) 0 K.
- (ii) Given the intensity relationships above, which way would we do the experiment with the sample at (a) room temperature, (b) liquid helium temperature ?

E8.

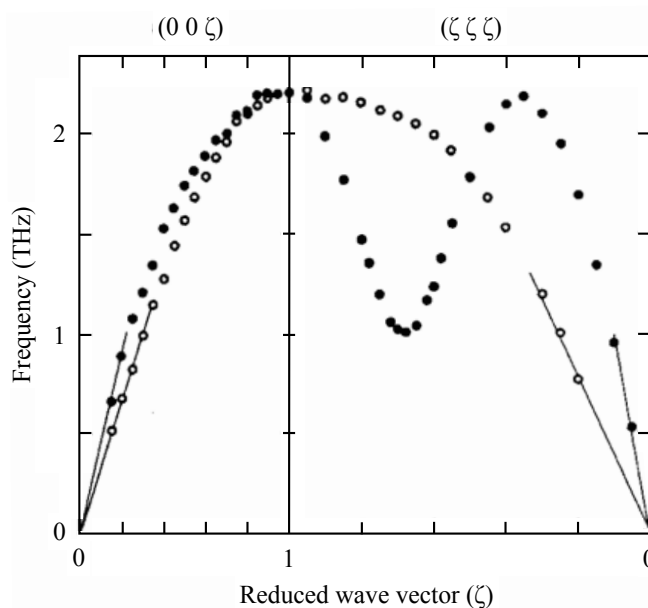
Is it possible to measure the $TA[00L]$ phonon around the 440 reciprocal-lattice point ?

To map out the dispersion curves in Figure E4, we would do energy scans, say from 2 to 8 meV, at a series of \mathbf{q} values between $[220]$ and $[221]$. A single peak would appear on each scan, giving the phonon energy for that reduced wave-vector.

E9.

Suppose an experiment is performed to measure the phonon dispersion curves of potassium on a three-axis spectrometer, when the energy of the beam scattered into the analyser is held fixed at 3.5 THz. For a measurement of the LA mode at $\mathbf{Q} = [2.5, 0, 0]$, what will be the energy of the incident beam for an experiment in which the neutron beam loses energy in the creation of a phonon. The phonon dispersion curves of potassium are given in Fig. E9, and the lattice parameter of potassium is 5.23 Å.

Figure E9. Acoustic mode dispersion curves for potassium (bcc) measured by inelastic neutron scattering. (Data taken from Cowley et al. *Phys. Rev.* **15**, 487, 1966.)



F. Magnetic Neutron Scattering

F1. Derive the expression for the convolution of two Gaussians.

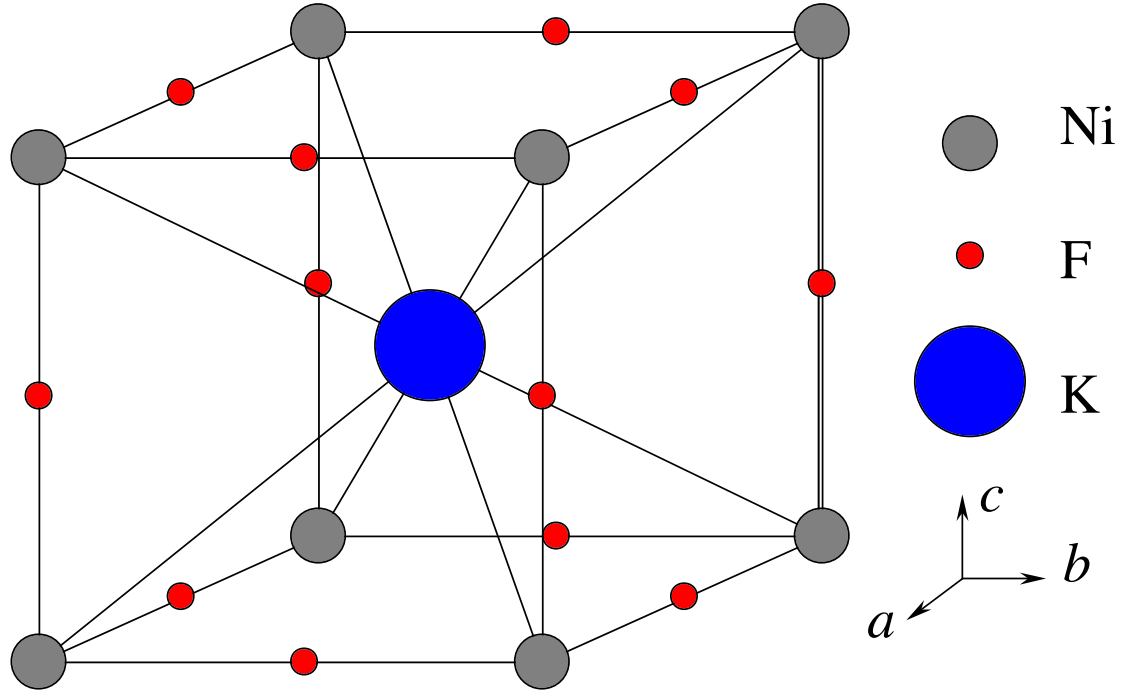


Figure F1: *The cubic perovskite structure of KNiF_3*

F2. KNiF_3 has a cubic perovskite structure, shown in Figure F1. It becomes antiferromagnetic below a Néel temperature of $T_N = 275$ K. In this magnetic structure, the magnetic moments lie along the edges of the cube. Each moment is antiferromagnetically coupled to its nearest neighbour.

Start by assuming that the material has a single magnetic domain and that the magnetic moments point along c .

2.1 Draw the magnetic unit cell in real space.

2.2 Draw the nuclear reciprocal lattice plane spanned by $[110], [001]$ from $-2 \leq h, k, l \leq 2$

2.3 Superimpose on this the magnetic reciprocal lattice. Index the magnetic points with the magnetic reciprocal lattice units.

2.4 Write the magnetic structure factor for the magnetic peaks. Will all the peaks have the same intensity? If not, why not? What implication does this have for the symmetry of the magnetic lattice?

F3. KNiF_3 is said to be an excellent example of a Heisenberg antiferromagnet. This means that it will have almost no anisotropy and the spin waves between the Brillouin zone centres will resemble something like in figure D2.

Assume that the spin waves can be described using a classical picture (i.e. magnetic moments precessing on cones). Identify the Brillouin zone centres along the $[001]$ and $[110]$ axes. Will spin waves be measurable along these directions? If yes, how will the intensities compare?

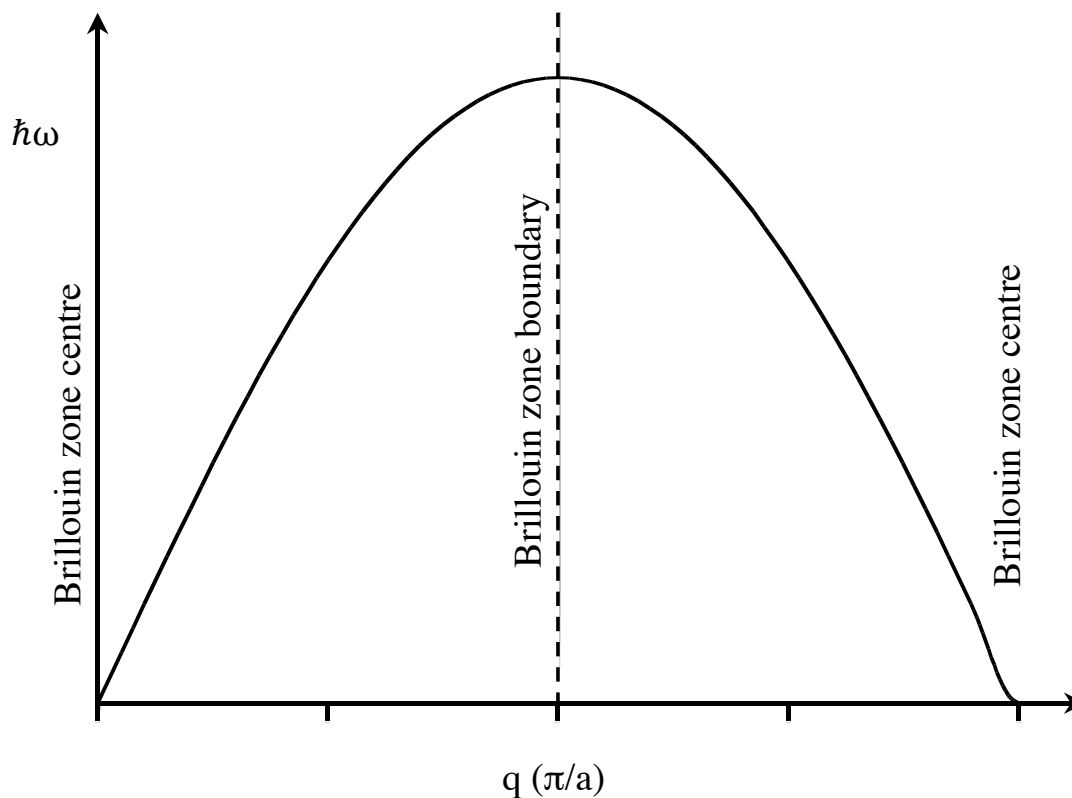


Figure F2: Schematic showing a spin wave dispersion from a Heisenberg antiferromagnet.

F4. Now assume that the sample has many domains. What will happen to the intensities of the Bragg peaks and the inelastic scattering?

G. Disordered Materials Diffraction

G1.

The interatomic potential, the pair distribution function, the coordination number, and the structure factor. (N.B. To do this exercise it is helpful to have access to a computer spreadsheet.)

Typically atomic overlap is prevented by strong repulsive forces that come into play as soon as two atoms approach one another below some characteristic separation distance σ (which is usually expressed in units of $\text{\AA} = 10^{-10} \text{ m}$). At greater distances the atoms are normally attracted to one another by weak van der Waals (dispersion) forces, the magnitude of which is governed by an interaction parameter ϵ , which can be expressed in units of kJ per gm mole.

These facts can be conveniently (but only approximately) expressed by the model Lennard-Jones potential energy for two atoms separated by a distance r :

$$U(r) = 4\epsilon \left(\left(\frac{\sigma}{r} \right)^{12} - \left(\frac{\sigma}{r} \right)^6 \right) \quad (\text{G1.1})$$

The radial distribution function (RDF), normally written $g(r)$ and also called the pair distribution function (PDF), describes the relative density of atoms (compared to the bulk density) of atoms a distance r from an atom at the origin.

G1.1 The pair potential.

a) With $\epsilon = 0.6 \text{ kJ/mole}$ and $\sigma = 3.0 \text{\AA}$, sketch this function approximately in the distance range $0 - 10 \text{\AA}$.

b) What do the values of ϵ and σ signify?

c) Mark on your graph the repulsive core and dispersive regions.

G1.2 Low density limit.

According to the theory of liquids (see for example Theory of Simple Liquids, J P Hansen and I R McDonald, 2nd Edition, Academic Press, 1986), in the limit of very low density (e.g. like the density of the air in the atmosphere), the PDF between atom pairs is given by the exact expression:

$$g_{\text{low}}(r) = \exp \left[- \frac{U(r)}{k_B T} \right] \quad (\text{G1.2})$$

where k_B is Boltzmann's constant. In the units of kJ per mole $k_B = 0.008314 \text{ kJ/mole/K}$.

a) Sketch this function for the Lennard-Jones potential used in G1.1 a) at (say) $T = 300\text{K}$. $g(r)$ is the primary function which is being measured in a diffraction experiment.

b) From your sketch, describe briefly the main differences between $U(r)$ and $g(r)$.

c) Describe qualitatively what would happen to $g_{\text{low}}(r)$ for example if you increased ϵ by a factor of 2, or increased σ by 20%?

Note that in the limit of zero density $g_{\text{low}}(r)$ does not go to zero.

G1.3 High densities.

Of course real materials occur with much higher densities than those of low density gases. This gives rise to an additional contribution to $g(r)$ from three-body and higher order correlations. In general these are difficult or impossible to calculate analytically, so that resort has to be made to computer simulation to estimate the effect of many body correlations.

Figure G1.1 shows a simulated $g(r)$ for our “Lennard-Jonesium” of G1.1, at two densities, (a) $\rho = 0.02$ and (b) $\rho = 0.035$ atoms/ \AA^3 respectively.

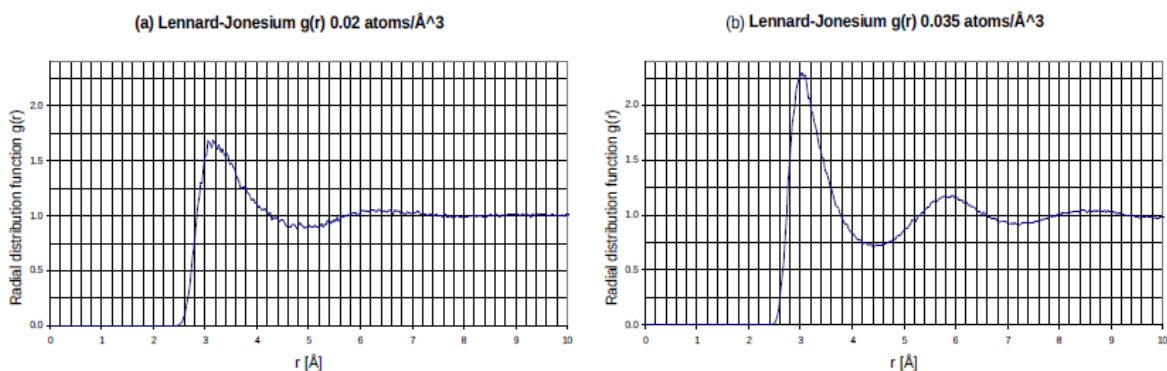


Figure G1.1

a) Comparing these with your “zero density” sketch of $g(r)$ from G1.2, describe the main effects of many-body correlations on $g(r)$. In particular:-

- i) How does the position of the first peak move with the change in density?
- ii) How do the positions of the second and subsequent peaks move with change in density?
- iii) Is the amount of peak movement what you expect based on the density change?

b) Why do you think many-body correlations have the effect they do?

G1.4 Coordination numbers

These are defined as the integral of $g(r)$ in three dimensions over a specified radius range:-

$$N(R_1, R_2) = 4\pi\rho \int_{R_1}^{R_2} r^2 g(r) dr \quad (\text{G1.3})$$

The “running” coordination number at radius r is defined as $N(0, r)$, which is sometimes written simply as $N(r)$. Figure G1.2 shows the running coordination numbers for the RDFs of Figure G1.1

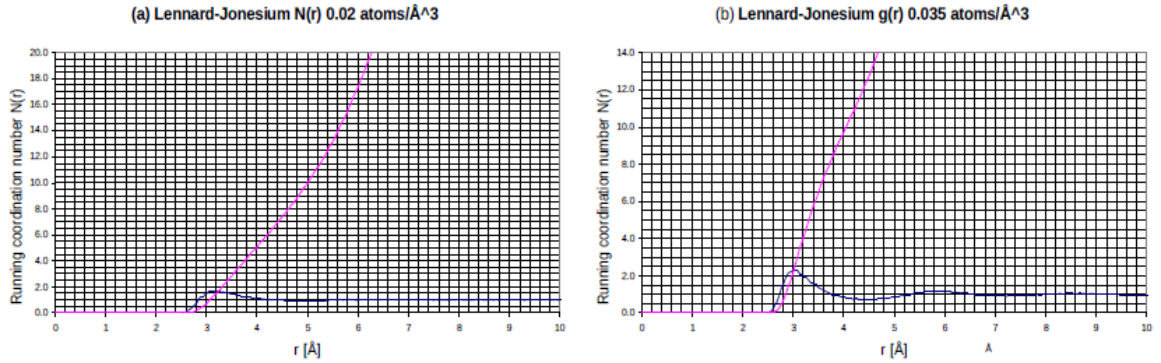


Figure G1.2

a) Using the grid provided estimate approximately the coordination number up to the first minimum in $g(r)$ for each of the cases shown in Figure G1.1. This is what is frequently quoted as the “coordination number” of the atom at each density. Do these numbers scale with the density?

b) If instead we had used the same distance range for both densities would the coordination numbers scale with density?

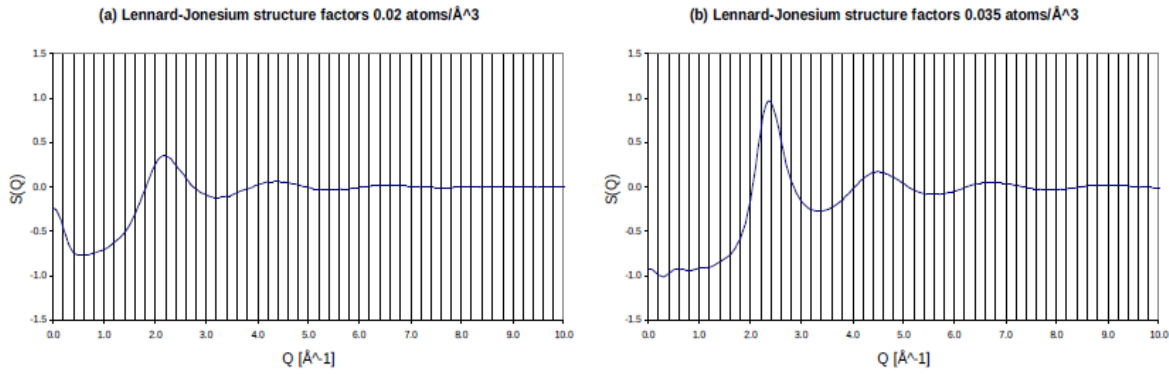
G1.5 The structure factor.

The diffraction experiment does not measure $g(r)$, but its Fourier transform, the structure factor, $H(Q)$, where

$$H(Q) = 4\pi\rho \int_0^{\infty} r^2 \left(g(r) - 1 \right) \frac{\sin Qr}{Qr} dr \quad (\text{G1.4})$$

where Q , the wavevector transfer in the diffraction experiment, is given by, $Q = 4\pi \sin \theta / \lambda$, with 2θ the detector scattering angle, and λ the radiation wavelength.

The structure factors corresponding to the two densities of Lennard-Jonesium in G1.3 are shown in Figure G1.3.



- Describe the effect of changing the density on the structure factor. How does this compare with effect of changing the density on the radial distribution function?
- What is the (approximate) relationship between the position of the first peak in $g(r)$ and the first (primary) peak in $H(Q)$?
- What would happen to the position of the first peak in $H(Q)$ if we increased the value of σ ?
- Given that the radial distribution function remains finite at all densities, using Eq. G1.4 what is the structure factor of an infinitely dilute gas?

G 2.

Two component systems: use of isotope substitution and the case of molten ZnCl_2 .

The diffraction pattern from a system containing 2 atomic components can be written as

$$F(Q) = c_1^2 \langle b_1 \rangle^2 H_{11}(Q) + 2c_1 c_2 \langle b_1 \rangle \langle b_2 \rangle H_{12}(Q) + c_2^2 \langle b_2 \rangle^2 H_{22}(Q) \quad (\text{G2.1})$$

where c_α is the atomic fraction and b_α is the neutron scattering length of component α , $H_{\alpha\beta}(Q)$ is the partial structure factor (psf), analogous to (1.4) above, for the pair of atoms α, β , defined by:

$$H_{\alpha\beta}(Q) = 4\pi\rho \int_0^\infty r^2 \left(g_{\alpha\beta}(r) - 1 \right) \frac{\sin Qr}{Qr} dr \quad (\text{G2.2})$$

and $g_{\alpha\beta}(r)$ is the site-site radial distribution function of β atoms about α . The brackets around the scattering lengths indicate that the scattering lengths have to be averaged over the spin and isotope states of each atomic component. The coordination number of β atoms about atom α can be defined in an analogous manner to Eq. G1.3

$$N_{\alpha\beta}(R_1, R_2) = 4\pi\rho c_\beta \int_{R_1}^{R_2} r^2 g_{\alpha\beta}(r) dr \quad (\text{G2.3})$$

A general rule is that if there are N distinct atomic components in a system, then there are $N(N+1)/2$ site-site radial distribution functions and partial structure factors to be determined. By “distinct atomic components” we do not necessarily mean atom types. For example a methyl hydrogen atom on an alcohol molecule is distinct from the point of view of the structure to a hydroxyl hydrogen atom, even though they are the same atom type.

G2.1 A classic example of the application of the isotope substitution method to a two-component liquid is the molten ZnCl_2 experiment of Biggin and Enderby (J. Phys. C: Solid State Phys., 14, 3129-3136 (1981)).

- a) What are the atomic fractions of Zn and Cl in ZnCl_2 salt?
- b) Hence, based on Eq. G2.1, write down a formula for the diffraction pattern of ZnCl_2 in terms of the Zn-Zn, Zn-Cl and Cl-Cl partial structure factors.
- c) Given that two isotopes of chlorine are available, ^{35}Cl and ^{37}Cl , with markedly different scattering lengths (11.65fm and 3.08fm respectively) briefly explain how you might extract the three partial structure factors for ZnCl_2 experimentally.
- d) Are there any other experimental techniques that could be used to do this?

G2.2 Figure G2.1 shows the actual diffraction data of Biggin and Enderby, while Table GI below lists the neutron weights outside each partial structure factor for each of the Biggin and Enderby samples:

Sample	At% ^{35}Cl [%]	At. % ^{37}Cl [%]	Individual psf weighting factors [barns/sr/atom] [†]		
			Zn-Zn	Zn-Cl	Cl-Cl
Zn $^{35}\text{Cl}_2$	99.3	0.7	0.0358	0.2929	0.5982
ZnMixCl $_2$	67.7	32.3	0.0358	0.2253	0.3541
Zn $^{37}\text{Cl}_2$	2.7	97.3	0.0358	0.0837	0.0489

Table GI

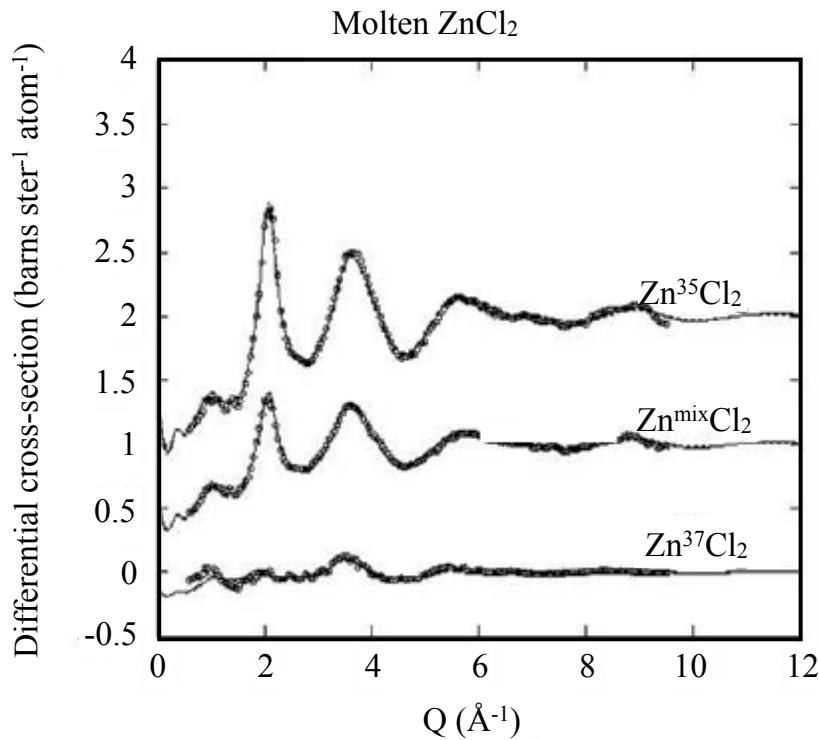


Figure G2.1 Diffraction data (points) for molten zinc chloride using different mixtures of chlorine isotopes. The line is a modern fit to these data using an EPSR (empirical potential structure refinement) computer simulation.

- a) On the basis of the numbers in this table describe any problems that might arise in attempting to invert the diffraction data to partial structure factors. Look also at the diffraction data themselves, in Figure G2.1.
- b) Given those reservations, what might happen when we try to convert the extracted partial structure factors to radial distribution functions using the inverse Fourier transform:

$$g_{\alpha\beta}(r) = 1 + \frac{1}{2\pi^2\rho} \int_0^{\infty} Q^2 H_{\alpha\beta}(Q) \frac{\sin Qr}{Qr} dQ \quad (\text{G2.4})$$

- c) Describe another method that might be used to separate out the site-site radial distribution functions from the measured diffraction data.

G2.3 Figure G2.2 shows a computer simulation of the radial distribution functions and running coordination numbers of molten zinc chloride, ZnCl_2 , as derived from the Biggin and Enderby diffraction data.

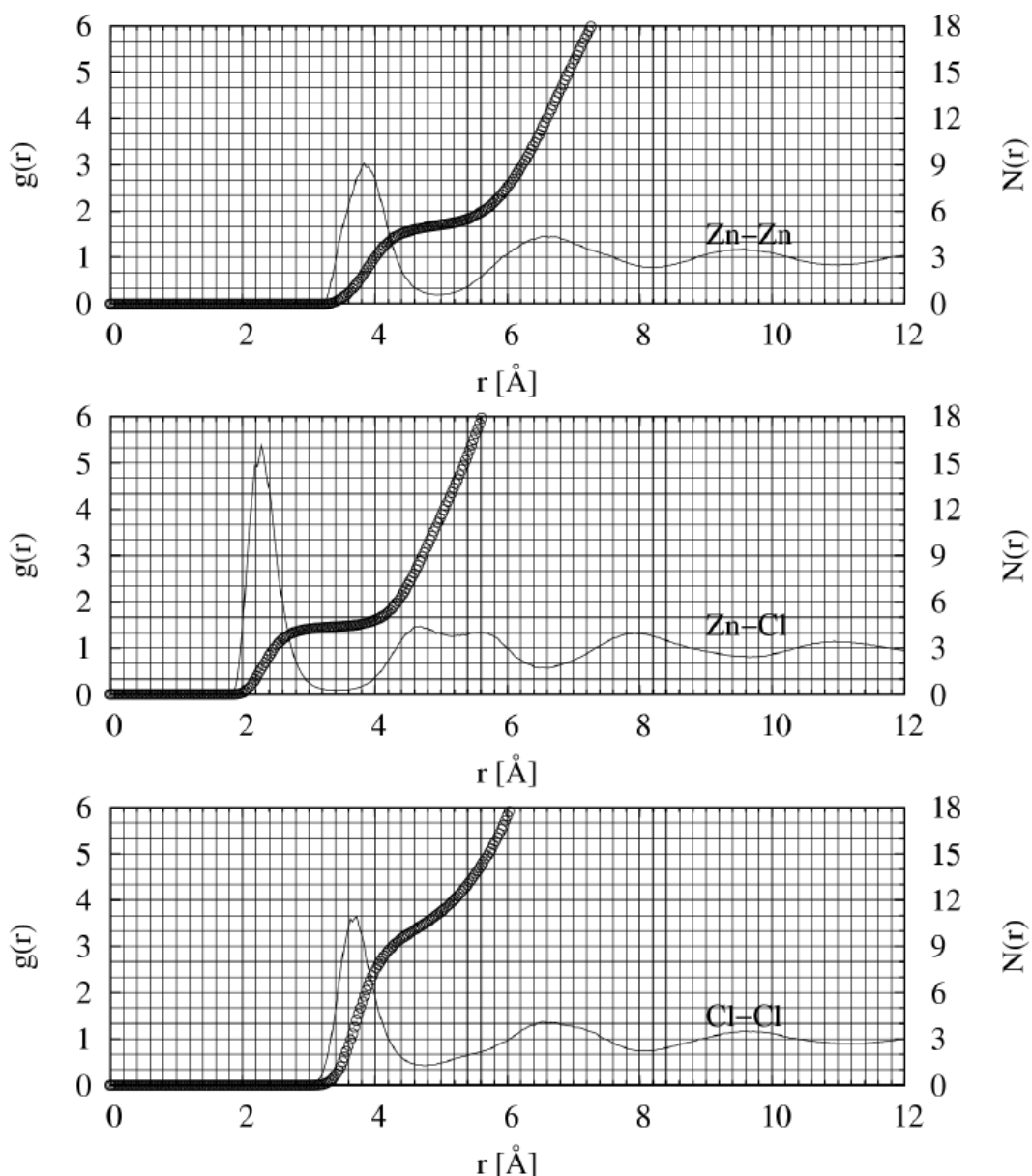


Figure G2.2 Radial distribution functions (lines, left-hand scale) and running coordination numbers (point, right-hand scale) for molten zinc chloride.

- Using the grid, or other method, estimate approximately the coordination number of Cl around Zn. What would be the corresponding coordination number of Zn around Cl?
- Given this number, and the position of the Zn-Zn and Cl-Cl first peaks, what can you say about the local structure in molten ZnCl_2 ?
- For the region beyond the first peaks, what do you notice about the three site-site rdfs for molten ZnCl_2 ? Use this to speculate on what might be happening to the ordering of the Zn and Cl atoms.

H: Polarized Neutrons

H1. a) A measurement of a Si Bragg peak using the instrument in Fig. H1, give 51402 counts/second with the flipper off and 1903 counts per second with the flipper on? What is: a) the Flipping Ratio, and b) the beam polarization? Provide also a calculation of the experimental uncertainty in these values.

b) What would be the main sources of systematic error in this measurement?

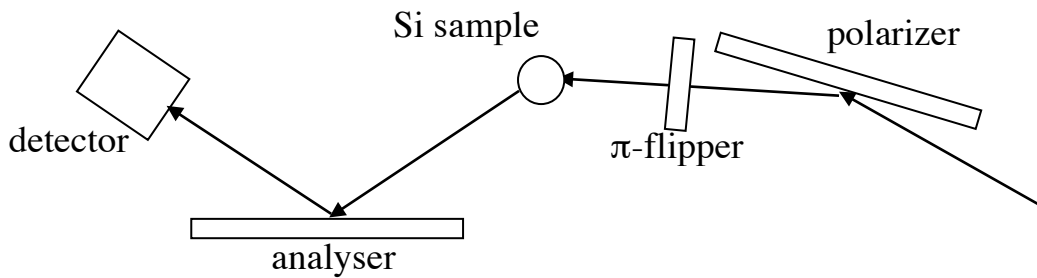


Figure H1

H2. a) Fig. H2 shows a configuration for a Dabbs-foil (current sheet) flipper, designed for neutrons of wavelength 2 \AA . A current I flows vertically along the foil, giving rise to a horizontal field $B_F = 3 \text{ mT}$. The overall guide field B_G – also equal to 3 mT – is cancelled at the foil position by correction coils. The overall distance between the purely vertical guide field regions is 20 cm . By checking the rate of the field rotation, state whether you believe that this is a good design for a π -flipper.

[Hint: *The neutron gyromagnetic ratio, γ_n , is the ratio of the neutron magnetic moment to its angular momentum, i.e.: $\gamma_n = \mu_n / \frac{1}{2}\hbar = 1.83 \times 10^8 \text{ rad. s}^{-1} \text{ T}^{-1}$]*

b) Suggest ways in which the design may be improved.

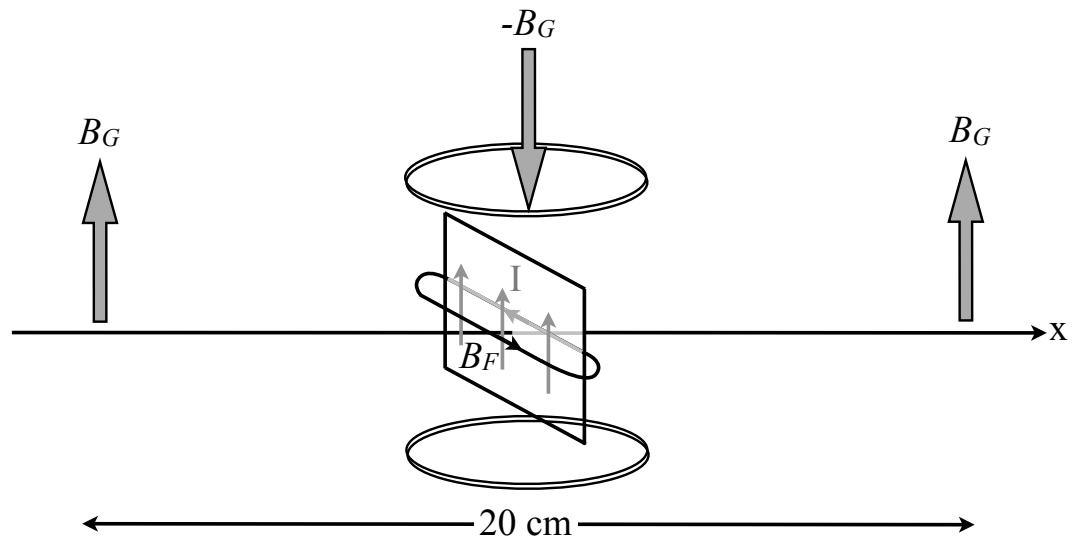


Figure H2: Design for a Dabbs' Foil π -Flipper

- H3.** a) Assuming that a polarizing filter has an absorption cross-section consisting of a spin-dependent part and a spin-independent part of the form

$$\sigma_{\pm} = \sigma_0 \pm \sigma_p$$

show that the neutron polarization and transmission through the filter are given by

$$P = -\tanh(\sigma_p Nt), \text{ and } T = \exp(-\sigma_0 Nt) \cosh(\sigma_p Nt)$$

[Hint: the number of neutrons transmitted through the filter will be proportional to $\exp(-N\sigma t)$ where N is the number density of scatterers in the filter, and t is the thickness]

- b) Show that the polarization of the ^3He nuclei is given by:

$$P_{\text{He}} = -\frac{\sigma_p}{\sigma_0},$$

and hence find expressions for the polarization and transmission of a ^3He spin-filter.

[Hint: use the expression $\sigma_{\pm} = \sigma_0(1 \mp P_{\text{He}})$ for the absorption of ^3He gas of polarization P_{He}]

H4. a) Show that the polarizing efficiency of a crystal monochromator is given by

$$P = \frac{2F_N F_M}{F_N^2 + F_M^2},$$

where the symbols have their usual meanings.

b) By expressing the polarization as a function of the ratio of structure factors, show that the maximum polarization is obtained when the nuclear and magnetic structure factors are equal in magnitude.

H5. Why is it not necessary to analyse the neutron spin when scattering from a ferromagnet saturated in a direction perpendicular to \mathbf{Q} ?

H6. a) Verify the following relations (so-called Pauli spin relations):

$$\begin{aligned}\sigma_x |\uparrow\rangle &= |\downarrow\rangle, & \sigma_x |\downarrow\rangle &= |\uparrow\rangle \\ \sigma_y |\uparrow\rangle &= i|\downarrow\rangle, & \sigma_y |\downarrow\rangle &= -i|\uparrow\rangle \\ \sigma_z |\uparrow\rangle &= |\uparrow\rangle, & \sigma_z |\downarrow\rangle &= -|\downarrow\rangle\end{aligned}$$

where σ_x , σ_y and σ_z are the Pauli spin matrices and the spin-up and spin-down (along z) eigenstates are given by $|\uparrow\rangle = \begin{pmatrix} 1 \\ 0 \end{pmatrix}$ and $|\downarrow\rangle = \begin{pmatrix} 0 \\ 1 \end{pmatrix}$

b) Hence, by calculating the magnetic neutron scattering potential:

$$V_m = \frac{-\gamma_n r_0}{2m_n} \sum_{\xi} \sigma_{\xi} M_{\perp \xi}$$

for each spin-state transition show that the spin flip scattering is sensitive only to those components of the magnetisation \mathbf{M}_{\perp} perpendicular to the neutron polarization vector (along z).

H7. Using the Moon, Riste and Koehler expressions, together with the definition of the Fourier component of the magnetisation perpendicular to \mathbf{Q} , \mathbf{M}_{\perp} , show that the magnetic scattering is entirely spin-flip if the neutron polarization is parallel to \mathbf{Q} .

H8. What is the advantage of the X-Y-Z difference method of magnetic scattering separation over the method of measuring with the neutron polarization $\mathbf{P} \parallel \mathbf{Q}$?

I. High resolution spectroscopy (TOF, backscattering and Spin-Echo)

The aim of this section is to get a feeling for the energy resolution of different spectrometer types: time-of-flight (TOF), backscattering (BS) and spin echo (NSE) spectrometers.

All the following calculations assume a **neutron wavelength of $\lambda=6.3 \text{ \AA}$** .

Planck's constant is $h=6.6225 \cdot 10^{-34} \text{ Js}$, sometimes usefully expressed as $h = 4.136 \text{ \mu eV ns}$. Neutron mass $m_n=1.675 \cdot 10^{-27} \text{ kg}$.

I1.

Calculate the neutron speed v_n in [m/s] and the neutron energy in μeV .

$v_n =$ _____ m/s; $E_n =$ _____ μeV .

I2. - Time-of-flight spectroscopy

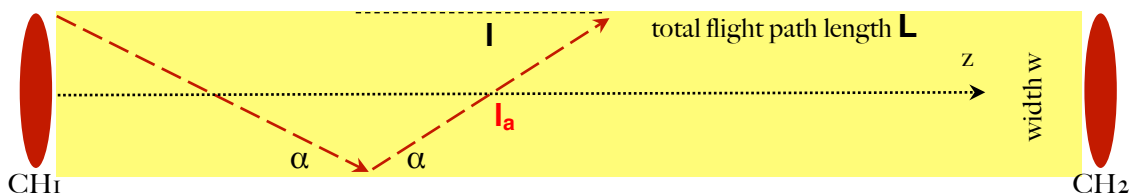


Figure I1 *Time-of-flight spectrometer with two choppers CH_1 and CH_2 separated by a distance L*

All contributions to the energy resolution in time-of-flight can be formulated as time uncertainty $\Delta t/t$. We consider only the primary spectrometer (before sample) and aim for an energy resolution better than $1\mu\text{eV}$.

a) Show first that $\Delta E/E = 2\Delta t/t$ (express E as fct. of v and assume $\Delta d = 0$):

$E =$ _____ and with $\Delta d = 0$:

$\Delta E =$ _____, which results in $\Delta E/E =$ _____.

Several contributions add to the neutron flight time uncertainty Δt . To simplify, let's consider a chopper spectrometer with flight path L between two choppers as sketched in the Figure. I1. and let's first look at neutrons flying parallel to z .

b) Calculate the flight time along path $L = 100$ m: $T_0 \sim$ _____ s.
 If we want to get an energy resolution of $1 \mu\text{eV}$, this corresponds to $\Delta E/E \sim$ _____ for 6.3 \AA neutrons.

This can give us an idea for the maximum allowed flight time difference along L : $\Delta E/E_0 * T_0/2 \sim$ _____ μsec

c) Path difference in neutron guide

For the reflected neutrons estimate the max. flight path differences in a super-mirror guide with $m=2$ coating and width w . The critical angle α (maximal reflection angle = half divergence) in such a guide is $\alpha \sim 0.1^\circ$ m
 $\lambda =$ _____ $^\circ$.

Estimate the flight path difference with respect to neutrons which fly parallel. One way is to show that $\Delta L/L = (1/\cos \alpha) - 1$ and thus:

$\Delta L/L =$ _____ $= \Delta t/t$ and therefore:

$\Delta E/E \sim$ _____.

We prove this by referring to Fig. I.1:

$l =$ _____;

$l_a =$ _____;

$l_a / l =$ _____ independent of w ; if n is the number of reflections, then we can write the full path difference as:

$\Delta L = n*(l_a-l) =$ _____

and thus $\Delta L/L = (1/\cos \alpha)-1$.

d) Chopper Opening Time

Another contribution is the chopper opening time which leads to a spread in neutron velocity and thus to flight time differences dt . In order to reach similar $\Delta t/t = \Delta v/v$ as above one needs fast rotating choppers delivering short pulses.

If CH1 releases at $t = 0$ an arbitrarily sharp pulse of a white beam, then the CH2 delay T selects a neutron velocity v_0 and the CH2 opening time determines $\Delta v/v$.

We want again $1\mu\text{eV}$ energy resolution therefore we need

$$\Delta v/v_0 = \Delta t/T = \underline{\hspace{2cm}}.$$

The chopper opening time must then be

$$\Delta t_{\text{CH2}} < 1/2 * (1\mu\text{eV}/E_0) * v_0 = \underline{\hspace{2cm}} \text{ [s/m]} * L \text{ [s]}.$$

Mechanically, the chopper opening time is defined as: $\Delta t_{\text{CH2}} = \beta / 360 / f$, where β is the chopper window angular opening and $\beta/360$ is the duty cycle (which equals the fraction of neutrons transmitted by the chopper). We see that this condition can be achieved by increasing the flight path (or by decreasing v_n), by increasing the chopper frequency or by narrowing the chopper window (intensity loss).

Choosing a duty cycle of 0.01 one needs a very long flight path between CH1 and CH2 of $L=100\text{m}$ and a high chopper frequency of

$$\underline{\hspace{2cm}} \text{ Hz} = \underline{\hspace{2cm}} \text{ rpm}$$

to reach $1\mu\text{eV}$ energy resolution.

This condition becomes more restrictive if we consider the finite opening time of the first chopper as well. Finally, we mention that all the contributions in the primary and secondary spectrometer have to be added in quadrature:

$$\Delta t/t = \text{sqrt}[(\Delta t_1/t_1)^2 + (\Delta t_2/t_2)^2 + \dots]$$

Additional choppers are usually needed to avoid frame overlap and harmonics, which reduces the intensity further. To achieve a $1\mu\text{eV}$ energy resolution by TOF is technically demanding (choppers), expensive (guides) and low in flux. Thus TOF-chopper-instruments have typically energy resolutions $> 10 \mu\text{eV}$. ex.: IN5 at 6.3\AA has roughly $40 \mu\text{eV}$ energy resolution.

Increasing λ helps but reduces the maximum Q . Calculate the elastic Q for 3\AA , 6\AA and 15\AA neutrons, assuming a maximum scattering angle of 140° :

$$Q = \underline{\hspace{2cm}} = \underline{\hspace{2cm}} \text{\AA}^{-1}, \underline{\hspace{2cm}} \text{\AA}^{-1} \text{ and } \underline{\hspace{2cm}} \text{\AA}^{-1}$$

I2. - Backscattering spectroscopy

Reactor backscattering spectrometers are based on perfect crystal optics. High energy resolution is achieved by choosing Bragg angles Θ as close as possible to 90° . Two major terms determine then the energy resolution: the spread in lattice spacing $\Delta d/d$ of the monochromator and the angular deviation ε from backscattering direction (the latter includes the beam divergence α if considered as $\varepsilon = \alpha/2$).

Write down the Bragg equation (neglecting higher orders):

_____ or equivalently using $k=2\pi/\lambda$ and $\tau = 2\pi/d$
(reciprocal lattice vector of the Bragg reflection): _____.

Deduce the wavelength resolution $\Delta\lambda/\lambda$ by differentiating the Bragg equation:

$\Delta\lambda =$ _____ $+$ _____ and thus

$\Delta\lambda/\lambda =$ _____ $+$ _____, or equivalently:

$\Delta k =$ _____ $+$ _____ and thus

$\Delta k/k =$ _____ $+$ _____.

The energy resolution is given by two terms. The first one, $\Delta d/d = \Delta\tau/\tau$, can be calculated by dynamical scattering theory as $\Delta\tau/\tau = h^2/m 4 F_\tau N_c$, where F_τ is the structure factor of the reflection used and N_c the number density of atoms in the unit cell. The second one, the angular deviation, can for $\Theta \approx 90^\circ$ be expanded in powers of Θ and contributes approximately as $\Delta\lambda/\lambda \sim \Delta\Theta^2/4$ ($\Delta\Theta$ in radians).

Calculate now the contribution to the energy resolution of both terms for a perfect crystal Si(111) monochromator (6.271Å, but approximate by 6.3Å as above).

With $F_{\tau=(111)}$ and N_c for Si(111) the extinction contribution for Si(111) in backscattering is $\Delta d/d = 1.86 \cdot 10^{-5}$ and thus $\Delta E/E =$ _____ and $\Delta E =$ _____ μeV .

Estimate the energy resolution contribution due to deviation from backscattering:

1) given by a sample diameter of 4 cm in 2 m distance from the analyser.

$\Delta E/E =$ _____, $\Delta E =$ _____ μeV

2) given by this sample at 1m distance:

$$\Delta E/E = \underline{\hspace{2cm}}, \Delta E = \underline{\hspace{2cm}} \mu\text{eV}$$

3) given by a detector being placed near backscattering, a sample - analyser distance of 1m and the distance sample center - detector center = 10cm below the scattering plane; the focus of the analyser sphere is placed in the middle between sample and detector:

$$\Delta E/E = \underline{\hspace{2cm}}. \Delta E = \underline{\hspace{2cm}} \mu\text{eV}$$

These examples show that for small enough deviations from BS energy resolutions of $< 1 \mu\text{eV}$ are easily achievable. Comparing this to TOF contributions above, it becomes clear that for a spallation source backscattering instrument, which combines TOF in the primary spectrometer with near-BS in the secondary spectrometer, it is very difficult to achieve sub- μeV resolution. The SNS BS (BASIS) instrument with 80m flight path has for example an energy resolution for Si(111) of $2.5 \mu\text{eV}$.

I3. - Neutron spin-echo spectroscopy

In neutron spin echo one uses the neutron spin which undergoes precessions in a magnetic field B. The precession angle ϕ after a path length L depends on the field integral, given by $\phi = \gamma * B * L / v_n$ (γ = gyromagnetic ratio of the neutron, v_n = neutron speed). For a polychromatic beam the precession angles of the neutron spins will be very different depending on the neutron speed and thus a previously polarized beam becomes depolarized. The trick is then to send the neutrons after the sample through a field with opposite sign and with the same field integral. Therefore, for elastic scattering, the precessions are “turned backwards”, again depending on the neutron velocity, and the full polarization is recovered. This allows the use of a wide wavelength band (range of incident neutron speeds) and therefore a high intensity which is ‘decoupled’ from the energy resolution.

In order to estimate a typically achievable energy resolution, we can calculate the longest time which is easily accessible in NSE.

The NSE time is given by: $t_{\text{NSE}} = \hbar \gamma B L / (m_n v_n^3)$ thus it is proportional to the largest achievable field integral $B * L$, which we take as 0.25 [T*m] .

Calculate the longest NSE time t_{NSE} for $\lambda = 6.3 \text{ \AA}$ neutrons (use v_n calculated above), knowing that $\gamma = 1.832 \cdot 10^8 \text{ [T}^{-1} \text{ s}^{-1}]$, $\hbar = 1.054 \cdot 10^{-34} \text{ J s}$; and $m_n = 1.675 \cdot 10^{-27} \text{ kg}$:

$$t_{\text{NSE}} = \underline{\hspace{2cm}} \text{ ns.}$$

Convert this time into an energy by multiplying its reciprocal value with $h=4.136 \mu\text{eV ns}$; we get: $E_{\text{NSE}} = \underline{\hspace{2cm}} \mu\text{eV}$.

For comparing measurements in time and in energy one often refers to Fourier-transformation which relates e.g. the characteristic relaxation time τ of an exponential relaxation in time to the width of a Lorentzian function in energy by $\tau = 1/\omega$. In spite of the fact that the relaxation time is usually smaller than the longest NSE time, converting the corresponding energy resolution by this relation gives:

$$E_{\tau} = \underline{\hspace{2cm}} \mu\text{eV} .$$

Because of $\tau < t_{\text{NSE}}$ and also because energy spectrometers can usually resolve better than the HWHM, the comparable resolution energy lies somewhere in between the two values calculated.

Note that the longest NSE time depends on wavelength λ as $t_{\text{NSE}} \propto \underline{\hspace{2cm}}$. Thus the resolution improves fast for increasing λ , but like calculated for the other spectrometers above, the maximum Q is reduced.

